SPACE WEATHER, VOL. 6, S05005, doi:10.1029/2007SW000354, 2008

Click Here for Full Article

Quantitative forecast of relativistic electron flux at geosynchronous orbit based on low-energy electron flux

Drew L. Turner[1,2] and Xinlin Li[1,2]

Received 27 July 2007; revised 18 December 2007; accepted 21 February 2008; published 23 May 2008.

[1] A strong correlation between the behavior of low-energy (tens to hundreds of keV) and high-energy (>1 MeV) electron fluxes measured at geosynchronous orbit has been discussed, and this correlation is further enhanced when a time offset is taken into account. A model has been developed incorporating this delay time between similar features in low- and high-energy electron fluxes to forecast the logarithm of daily averaged, 1.1–1.5 MeV electron flux at geosynchronous orbit several days in advance. The model uses only the current and previous days' daily averaged fluxes of low- and high-energy electrons as input. Parameters in the model are set by optimizing prediction efficiency (PE) for the years 1995–1996, and the optimized PE for these 2 years is 0.81. The model is run for more than one full solar cycle (1995–2006), and it consistently performs significantly better than a simple persistence model, where tomorrow's forecasted flux is simply today's value. Model results are also compared with an inward radial diffusion forecast model, in which the diffusion coefficient is a function of solar wind parameters. When the two models are combined, the resulting model performs better overall than each does individually.

Citation: Turner, D. L., and X. Li (2008), Quantitative forecast of relativistic electron flux at geosynchronous orbit based on low-energy electron flux, *Space Weather*, *6*, S05005, doi:10.1029/2007SW000354.

1. Introduction

1.1. Background

[2] Earth's radiation belts make up a significant part of the environment for many high-use orbits, such as those for low-Earth orbiting, GPS, geotransfer, and geosynchronous spacecraft. The relativistic electrons in the outer belt can be especially hazardous to spacecraft systems [e.g., *Baker et al.*, 1998; *Baker*, 2001], and thus, accurate forecasting of relativistic electron flux is important for mitigating the associated risk to spacecraft operations. This paper discusses a new, empirical model that forecasts the logarithm of daily averaged, 1.1–1.5 MeV electron flux at geosynchronous orbit (GEO).

[3] Having a good understanding of a system's governing physical processes enables one to more accurately forecast the system. There are currently many theories concerning the mechanisms that accelerate electrons in the outer radiation belt to relativistic energies, but so far, none has proven to be the dominant factor for all cases when compared with observational data. Early research found that the outer belt flux is driven by changes in the solar wind [*Williams*, 1966; *Paulikas and Blake*, 1979]. *Williams* [1966] showed that there was a 27-d periodicity (the same as the average solar spin period) in energetic electron intensities in the outer belt, and *Paulikas and Blake* [1979] found that MeV electron flux at GEO is enhanced 1–2 d after the passage of high-speed solar wind streams. However, changes in the solar wind alone do not account for the high variability of electron flux in the outer belt; relativistic electron flux can vary by up to 2 orders of magnitude over a timescale of hours to days. *Reeves et al.* [2003, p. 36-1] describe variability in electron flux resulting from geomagnetic storms as a "delicate and complicated balance between the effects of particle acceleration and loss." This "balance" of multiple magnetospheric source and loss processes, which often operate simultaneously, has been discussed in detail in reviews by *Li and Temerin* [2001], *Friedel et al.* [2002], and *Millan and Thorne* [2007].

1.2. Current Understanding

[4] Most source terms can be categorized into one of two types of models: (1) energization by radial transport and (2) local acceleration. Early theoretical work on radial transport, particularly inward radial diffusion, was conducted by *Fälthammar* [1965] and *Schulz and Lanzerotti* [1974]. This process involves a source population of particles in the outer magnetosphere, with a greater phase space density than in the inner magnetosphere, breaking the third adiabatic invariant and diffusing inward. By conserving the first adiabatic invariant, μ, particles are

[1]Laboratory for Atmospheric and Space Physics and Department of Aerospace Engineering Sciences, University of Colorado, Boulder, Colorado, USA.
[2]Also at Laboratory for Space Weather, Chinese Academy of Sciences, Beijing, China.

Copyright 2008 by the American Geophysical Union

energized to make up for the stronger magnetic fields encountered at lower L shells. Recent studies show that radial diffusion can be enhanced by ULF waves in the magnetospheric electric and magnetic fields [*Rostoker et al.*, 1998; *Hudson et al.*, 2000; *O'Brien et al.*, 2001, 2003; *Mann et al.*, 2004; *Sarris et al.*, 2006]. Another form of radial transport is that induced by impacts of interplanetary shocks with the magnetosphere, where the strong inductive electric fields transport a source population of particles, which also become energized in the process by conserving μ, to lower L shells [*Li et al.*, 1993, 2003; *Gannon et al.*, 2005].

[5] Electrons can also be accelerated to relativistic energies locally via wave-particle interactions, particularly whistler mode chorus [*Temerin et al.*, 1994; *Horne and Thorne*, 1998; *Summers et al.*, 1998; *Roth et al.*, 1999; *Meredith et al.*, 2002]. *Horne and Thorne* [1998] showed that whistler mode chorus could interact with electrons from a wide range of energy levels via Doppler-shifted cyclotron resonance and that it is theoretically possible to accelerate these seed populations up to relativistic (MeV) energies. *Bortnik and Thorne* [2007] provide a brief review of chorus' role in Earth's outer radiation belt dynamics and also define an "anchor point" at a few hundred keV, above which chorus tends to accelerate electrons and below which it tends to cause electrons to precipitate and be lost to the atmosphere. This is in accordance with *Summers et al.* [1998] and *Meredith et al.* [2002], who find that a seed population of electrons with energies of a few hundred keV can be significantly energized by interactions with chorus waves.

[6] A combination of both local acceleration and radial transport has also been used to explain the state of radiation belt energization, as mentioned by *O'Brien et al.* [2003] and *Onsager et al.* [2007]. *Brautigam and Albert* [2000] find that for the 9 October 1990 storm, radial diffusion is not enough to fully explain the observed increase in >1 MeV electron flux and suggest that wave-particle interaction with enhanced chorus waves may provide an explanation for the inconsistency. *Horne et al.* [2005] conclude that whistler mode chorus is a viable explanation for electron flux increases around L = 4.5 during geomagnetically active periods, while *Loto'aniu et al.* [2006] and *Barker et al.* [2005] show that inward radial diffusion can explain most of the observations during magnetic storms. *Selesnick and Blake* [2000] find that a local source of relativistic electrons may exist around L = 4 on the basis of phase space density calculations. *Green and Kivelson* [2004] go on to explain how a peak in phase space density at $L \approx 5$ could diffuse outward to account for the correspondence between flux enhancements at GEO and increased ULF wave power. Most recently, using a multisatellite study, *Chen et al.* [2007] find that, on average, electron phase space density peaks inside of GEO during storm times and nonstorm times alike, and they conclude that wave-particle interactions are the dominant source of relativistic electrons in the outer radiation belt. Therefore some local energization near the heart of the outer radiation belt may lead to a local peak in phase space density and radial diffusion. Those particles that diffuse inward gain energy but most likely interact with plasmaspheric hiss and are scattered into the loss cone [*Lyons et al.*, 1972; *Abel and Thorne*, 1998], while those particles that diffuse outward lose some energy but may retain enough to be measured as relativistic by satellites at GEO.

[7] Studies of electrons at various energies can provide some insight into acceleration and loss processes, which is crucial for better radiation belt models and forecasting abilities. *Li et al.* [2005] find that there is a good correlation between simultaneous electron flux measurements at various energy levels and that this correlation is enhanced when a time shift proportional to their energy difference is taken into account. They conclude that the time difference can be explained by either local energization, since it takes longer to energize electrons to higher levels, or radial diffusion, since lower-energy electrons diffuse faster than higher-energy electrons because there is more low-frequency ULF wave power available to drive lower-energy electrons through drift resonance. *Li et al.* [2005] also suggest that this time offset may be used as the basis for a forecast model.

1.3. Overview

[8] This paper's discussion of the current research begins with the results of a study similar to that of *Li et al.* [2005], investigating the offset correlation between low- and high-energy electron fluxes at GEO. These results are compared to the *Li et al.* [2001] predictive model, which solves the diffusion equation, calculating the diffusion coefficient as a function of solar wind parameters, to predict the logarithm of daily averaged relativistic electron flux at GEO. Recent improvements to the *Li et al.* [2001] model are also discussed briefly in section 2. A discussion of a newly developed model, which incorporates the delay time between low- and high-energy electron fluxes to forecast relativistic electron flux at GEO, follows in section 3. This new forecast model is then compared in section 4 to the *Li* [2004] forecast model, which is currently running online in real time and uses solar wind data to solve the diffusion coefficient, like the *Li et al.* [2001] model, to forecast daily averaged relativistic electron flux both 24 and 48 h in advance. A final model, which combines the new low- to high-energy model and the *Li* [2004] model, is then discussed and compared to the others individually. Section 5 provides a detailed discussion of the results and their implications, conclusions, and a brief note on proposed future work involving these models.

2. Data Handling and Fitting

[9] This study was conducted using Los Alamos National Laboratory (LANL) electron flux measurements from the synchronous orbit particle analyzer (SOPA) instruments on the LANL satellites at GEO. Hourly flux data from all available LANL satellites during the years 1995–

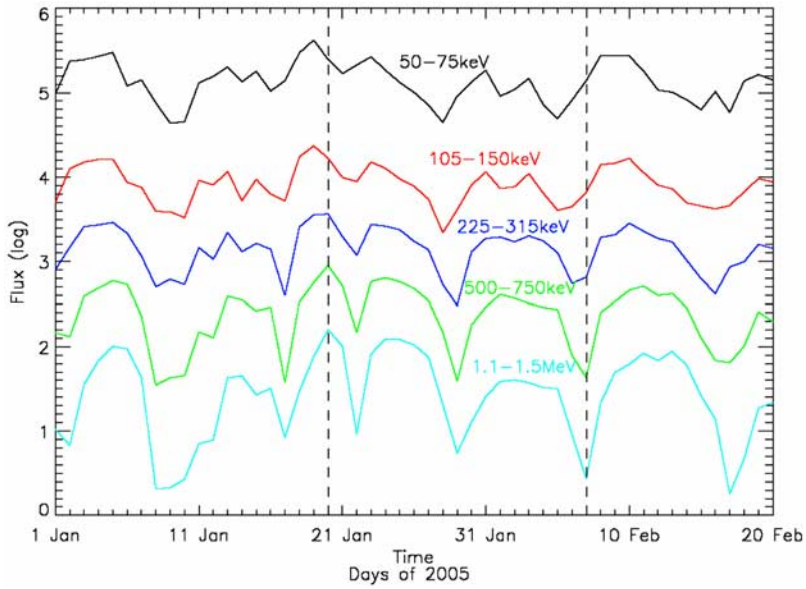

Figure 1. LANL logarithmic electron fluxes for various energy channels. Using dashed lines for constant time reference, it is noticeable how the lower-energy channels change before similar changes are seen in the higher-energy channels.

2006 are daily averaged to remove the variations observed at different local times in GEO. These variations arise from the spacecraft passing through different electron drift shells because of the asymmetry of Earth's magnetic field. At any given time, there were four to six point measurements from the LANL satellites, covering a wide range of local time. The local time flux dependence is discussed in detail by *Burin des Roziers and Li* [2006]. These daily averaged fluxes are used throughout the study as input for the models and also for comparison of model results to measured data. The LANL SOPA instrument measures differential electron flux on several channels covering different energy ranges. Figure 1 shows several of these channels for the first 2 months of 2005; the vertical dashed lines help display the time difference between similar features in the flux from various energy ranges. Notice how the 50–75 keV data often change more than a day before a similar change is seen in the 1.1–1.5 MeV data. *Li et al.* [2005] discuss this phenomenon in detail, and it is the basis for the forecast model discussed in this paper.

[10] As discussed by *Li et al.* [2005], the correlation between low- and high-energy electron fluxes is enhanced when a delay time is taken into account. Figure 2 shows correlation coefficients for various offset times in hours for the 50–75 keV and 1.1–1.5 MeV energy channels. Note that the optimum correlation coefficient occurs when the 1.1–1.5 MeV data set is shifted back by 37 h. This agrees with both what *Li et al.* [2005] found and what can be seen in Figure 1. Table 1 shows the linear correlation coefficients for all lower-energy channels compared to the 1.1–1.5 MeV energy channel for the years 1995–1996. Optimum offset times (in hours) are given in the second column. These offset times correspond to the maximum in the respective correlation versus offset time curves, of which Figure 2 is an example, and they represent the amount of time the 1.1–1.5 MeV energy channel should be shifted to produce the maximum correlation coefficient when compared to the lower-energy channels.

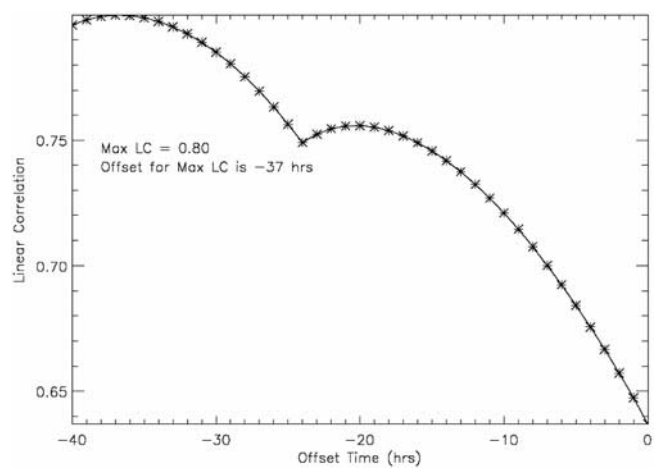

Figure 2. Linear correlation between 50–75 keV and 1.1–1.5 MeV energy channels for the years 1995–1996 for different offset times. Offset time is number of hours the 1.1–1.5 MeV data are shifted (back in time). Note that peak correlation, 0.80, occurs for a 37 h difference between the two channels. The kink at 24 h is an artifact of the daily averaged data.

Table 1. Correlations Between Low-Energy Channels and 1.1–1.5 MeV Channel for the Years 1995–1996[a]

Low-Energy Channel, keV	Optimum Offset, h	Linear Correlation Without Offset	Linear Correlation With Offset
50–75	−37	0.64	0.80
75–105	−35	0.69	0.82
105–150	−34	0.70	0.81
150–225	−17	0.73	0.80
225–315	−14	0.77	0.82
315–500	−11	0.82	0.85
500–750	−7	0.90	0.92
750–1100	−2	0.97	0.97

[a]Table shows how correlation between channels can be optimized when a time offset is taken into account. The third and fourth columns contain correlation coefficients for when no offset time (third column) and the optimum offset time (fourth column) are applied. The optimum offset time corresponds to the number of hours the 1.1–1.5 MeV channel is shifted back to produce the best linear correlation when compared to the lower-energy channel data.

[11] The *Li et al.* [2001] predictive model uses solar wind parameters to compute the diffusion coefficient and to numerically solve the one-dimensional radial diffusion equation. Model parameters are optimized for the years 1995–1996. Recently, a magnetopause-shadowing loss term was added. This new term results in the optimized prediction efficiency for 1995–1996 being improved from 0.81 to 0.82, which is a greater than 5% reduction in unpredicted variance. Linear correlation for both old and new forms of the model is 0.90. Prediction efficiency (PE) is defined as

$$\mathrm{PE} = 1 - \frac{\sum_i^n (m_i - p_i)^2}{\sum_i^n (m_i - \overline{m})^2}, \tag{1}$$

where m_i is the measured quantity, p_i is the predicted quantity, and $\overline{m}$ is the mean of all m_i. A PE of 0 means that, on average, the predicted values are equal to the average of the measured data set, and a PE of 1 means that the predicted values are all the same as the corresponding measured ones.

[12] On the basis of linear correlation, the potential for a model incorporating the time delay between low- and high-energy electron fluxes is good. From Table 2, one can see that with the 50–75 keV channel alone, a linear coefficient of 0.80 can be achieved when compared to the 1.1–1.5 MeV channel. This is not as good as the correlation of 0.90 achieved by the *Li et al.* [2001] model, but it demonstrates the potential effectiveness of using current lower-energy channel flux to predict flux at higher energies for some future time.

3. Forecast Model Description

[13] The new forecast model, which incorporates the time delay between low- and high-energy electron fluxes, is referred to throughout the remainder of this paper as either the low- to high-energy model or the low-e model and takes on the form of a simple source and loss differential equation (equation (2)), which physically implies that the flux variation depends on the balance of source and loss. This equation is numerically discretized (equation (3)) in order to solve for "tomorrow's" flux:

$$\frac{dj}{dt} = S + L \tag{2}$$

$$j(t + \Delta t)_{\mathrm{high}} = j(t)_{\mathrm{high}} + \Delta t(S + L), \tag{3}$$

where $j(t + \Delta t)_{\mathrm{high}}$ is tomorrow's average, high-energy flux; $j(t)_{\mathrm{high}}$ is "today's" average, high-energy flux; Δt is 1 d for a 24-h forecast; and S and L are the source and loss terms, respectively.

[14] S and L are determined by optimizing PE for the model for the years 1995–1996. The source and loss terms are initially a function of the data from today's 50–75 keV, 75–105 keV, 105–150 keV, and 1.1–1.5 MeV

Table 2. New Model Results Compared to Simple Persistence, *Li* [2004] Radial Diffusion, and a Combination of *Li* [2004] and the New Model[a]

	Run Years						
	1995–1996	1997–1998	1999–2000	2001–2002	2003–2004	2005–2006	1995–2006
Persistence 24-h PE	0.69	0.58	0.47	0.46	0.45	0.55	0.62
Low-e 24-h PE	0.81	0.73	0.63	0.54	0.66	0.74	0.73
Rad Diff 24-h PE[b]	0.84	0.72	0.63	0.53	0.64	0.75	0.74
Combo 24-h PE[c]	0.85	0.75	0.66	0.60	0.70	0.78	0.76
Persistence 48-h PE	0.34	0.07	−0.09	−0.12	−0.13	0.04	0.19
Low-e 48-h PE	0.59	0.39	0.24	0.27	0.29	0.36	0.46
Rad Diff 48-h PE[b]	0.67	0.36	0.27	0.12	0.30	0.48	0.46
Combo 48-h PE[c]	0.65	0.42	0.30	0.32	0.35	0.45	0.50

[a]Results are given for both 24 and 48 h forecasts. Models were run for 2 year increments from 1995 to 2006 (second through seventh columns) as well as for the full 12 years at once (eighth column).
[b]Rad Diff, radial diffusion.
[c]Combo, combination of *Li* [2004] and the new model.

energy channels as well as "yesterday's" 1.1–1.5 MeV energy channel, and weighting parameters for each are then adjusted on the basis of optimization. In this manner, if the inclusion of an energy channel's data does not lead to a better optimization result, its weighting factor is set to zero so that it is no longer part of the equation. The three lowest-energy channels are used to optimize the source term since they all change more than 24 h before the 1.1–1.5 MeV channel, which can be seen in Table 1. Low-energy fluxes are mapped to 1.1–1.5 MeV flux levels (see Figure 1 for general flux ranges for different energy channels) by using a power function, the parameters for which are also optimized for the years 1995–1996. The power function takes the form seen in the first term on the right side of the final form of the source term equation (equation (4)) where some constant (C_2) is raised to the power of the low-energy flux ($j(t - t_o)_{\mathrm{low}}$), which is raised to some other constant (b):

$$S = C_1 C_2^{\left(\frac{j(t-t_o)_{\mathrm{low}}}{j_o}\right)^b} + C_3 j(t - \Delta t)_{\mathrm{high}}, \quad (4)$$

where $j(t - t_o)_{\mathrm{low}}$ is today's low-energy flux; j_o is units of flux to nondimensionalize the exponent; $j(t - \Delta t)_{\mathrm{high}}$ is yesterday's high-energy flux; and C_1, C_2, C_3, t_o, and b are optimized parameters. This form of energy level conversion is similar to that used by *Burin des Roziers and Li* [2006] for their flux conversion to compare LANL differential flux at 1.1–1.5 MeV to GOES integral flux at >2 MeV. The low-energy flux is also interpolated and time shifted forward by t_o to best represent the time delay observed in the data. Also, adding yesterday's high-energy flux slightly improves the results. As mentioned previously, the pre-optimized form of the source equation incorporated flux from the three lowest-energy channels, but after optimizing the parameters, PE is best when S is simply a function of today's lowest-energy flux channel, 50–75 keV, and yesterday's high-energy (1.1–1.5 MeV) flux (equation (4)). In the final form of the loss equation, L is a function of today's high-energy flux:

$$L = -C_4 j(t)_{\mathrm{high}}, \quad (5)$$

where C_4 is another optimized parameter. Equation (5) simply implies that the more high-energy flux is present, the more there is to be lost. The optimized model parameters are $C_1 = 7.870 \times 10^{-4}$, $C_2 = 2.533$, $C_3 = 1.940 \times 10^{-2}$, $C_4 = 0.508$, $t_o = 6$ (hours), and $b = 1.927 \times 10^{-1}$. On the basis of these equations and parameters, tomorrow's 1.1–1.5 MeV forecasted flux is composed of today's 1.1–1.5 MeV flux (~49%), yesterday's 1.1–1.5 MeV flux (~2%), and today's 50–75 keV electron flux (~49%).

[15] One can see that this model includes persistence terms, $j(t)$ and $j(t - \Delta t)$, and this can make the results look as though there is sometimes a 1-d offset compared to the measured data. To help correct for the persistence offset, the gradient of today's and yesterday's high-energy logarithmic fluxes is used to either add to or subtract from tomorrow's forecast value. This employs the simple assumption that if the gradient between yesterday and today is positive, the flux is increasing and will continue to do so tomorrow, so a small amount, proportional to the gradient, is added to the forecast value. Likewise, if the gradient is negative, it is assumed that the flux will continue to decrease into tomorrow, and a small amount is subtracted from the forecast value. The gradient is calculated using the log of flux because the flux can change very drastically from one day to the next, and ultimately, the forecast is for the logarithm of flux. One more parameter, f, is added for this step, and it is also optimized for the years 1995–1996 and is set for the remaining years. The form of this corrective term is seen in equations (6) and (7):

$$g = \log_{10}\left[j(t)_{\mathrm{high}}\right] - \log_{10}\left[j(t - \Delta t)_{\mathrm{high}}\right] \quad (6)$$

$$\log_{10}\left[j(t + \Delta t)_{\substack{\mathrm{high}\\ \mathrm{corrected}}}\right] = \log_{10}\left[j(t + \Delta t)_{\mathrm{high}}\right](1 + fg), \quad (7)$$

where the left side of equation (7) is the final value for the forecast of the logarithm of the daily averaged 1.1–1.5 MeV flux; $j(t + \Delta t)_{\mathrm{high}}$ is tomorrow's flux calculated from equation (3); g is the gradient term; and f is the optimized multiplicative factor, which, after optimization, has a value of $f = 0.0625$. This term slightly improves the PE, ~1% for 1995–1996, by partially correcting for the persistence offset effect.

[16] Model parameters are set on the basis of the 1995–1996 optimization, and the model is then run for the years up to 2006 at 2 year intervals to demonstrate the model's effectiveness at forecasting future results given parameters that are set for some past time. The model is compared to the *Li* [2004] forecast model, which has been modified to run using the LANL 1.1–1.5 MeV data. A third model is created by combining the two. The combination model is discussed in more detail in section 4.

4. Model Results

[17] Using the parameters set for 1995–1996, the new model is run for 2 year periods from 1997 to 2006. Table 2 shows the results of the forecast model compared to a simple persistence model's results, where tomorrow's flux is simply the same as today's flux, as well as to the *Li* [2004] forecast model for both 24 and 48 h forecasts. Notice that both the new model's and the *Li* [2004] model's PEs are better than those of the simple persistence model for each 2 year period as well as for the full 12 year run (last column). PE for all models changes with the solar cycle; maximum PE occurs around the declining phase of the solar cycle, when high-speed solar wind streams are dominant (1995–1996 and 2005–2006), while minimum PE occurs around solar maximum (2001–2002). The *Li* [2004] model achieves a higher PE for the solar minimum

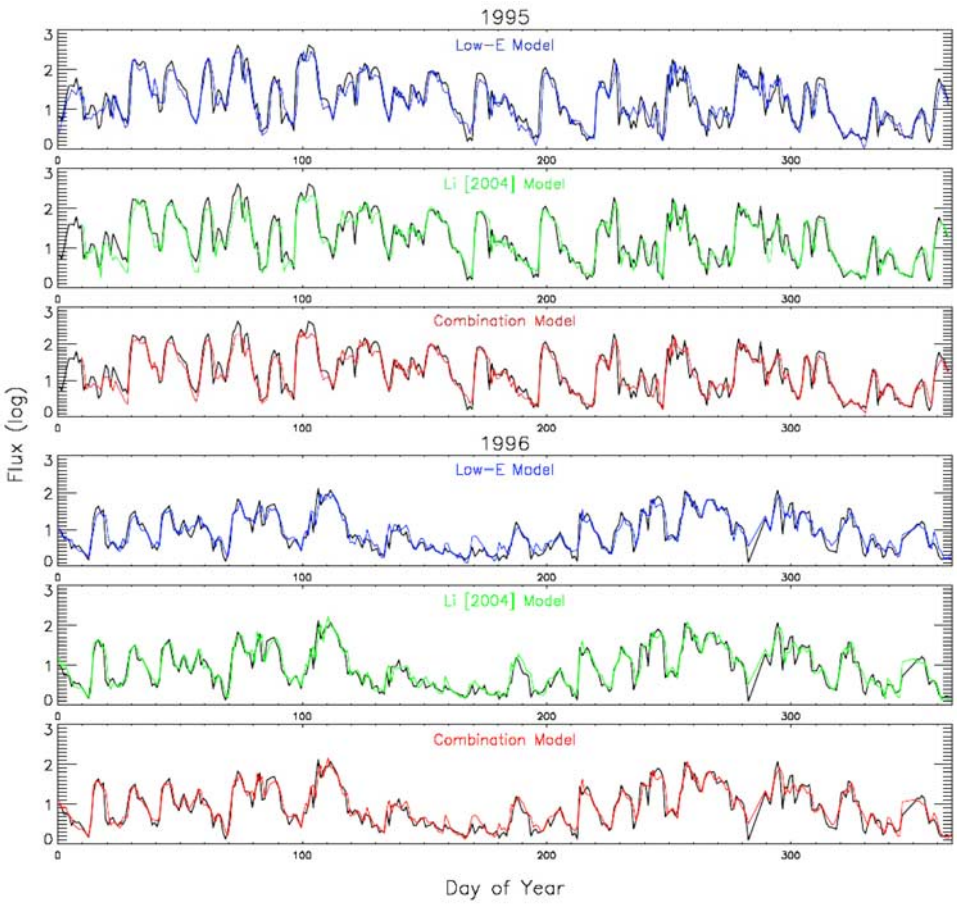

Figure 3. Various model results for the years 1995–1996. Top three plots are for 1995: daily averaged LANL 1.1–1.5 MeV measured electron flux (black) new low- to high-energy model (low-e, blue), *Li* [2004] radial diffusion model (green), and the new model combining both the low to high and *Li* [2004] models (red). The bottom three plots are in the same format for 1996.

years, while the new model is better during the solar maximum years. Figure 3 shows the results from both models for the years 1995–1996.

[18] The new low- to high-energy model has also proven effective at forecasting multiple days in advance. Another optimization was attempted to find new parameters for 48, 72, and 96 h forecasts, but PE turned out to be best when the 24 h forecast was simply projected forward to be compared with the measured values from each of these times. As expected, the PE gets worse as one forecasts further ahead in time, but the model forecast is consistently better than the simple persistence model using the measured data. Table 3 shows the results for the new model's multiday forecasts compared to the simple persistence model's multiday forecasts.

[19] A combination model has also been developed, which incorporates the *Li* [2004] forecasted flux into the low- to high-energy model by simply adding it, with its own weighting parameter, to the result from the new model. Using the same optimized forms of S and L seen in equations (4) and (5), parameters are optimized again for 1995–1996, and it is interesting to note that, as expected, the persistence term drops out of the low to high model terms (C_4 from equation (5) becomes 1.0 so that it cancels totally with the $j(t)_{\mathrm{high}}$ from equation (3)). This was expected since the *Li* [2004] model already incorporates persistence. This new form is seen in equation (8):

$$j_{\mathrm{combo}} = \tilde{j}(t + \Delta t)_{\mathrm{high}} + C_5 j_{\mathrm{Li}}, \tag{8}$$

where j_{combo} is the forecasted flux from the combined model, $\tilde{j}\ (t + \Delta t)_{\mathrm{high}}$ is the forecasted flux from the reoptimized low-e model, j_{Li} is the forecasted flux from the *Li* [2004] model, and C_5 is its weighting parameter. The new parameters for the combination model are $C_1 = 3.820 \times 10^{-4}$; $C_2 = 2.533$; $C_3 = 3.280 \times 10^{-2}$; $C_4 = 1.0$, $t_o = 6.0$; $b = 1.927 \times 10^{-1}$; and $C_5 = 0.703$, the new parameter multiplied by the *Li* [2004] forecasted flux. It is very interesting to note that this combination

Table 3. Comparing Multiple-Day Forecast Results From the Simple Persistence Model to the New Model[a]

Forecast Time, h	Simple Persistence PE	Low-E Model PE
24	0.69	0.81
48	0.35	0.59
72	0.06	0.33
96	−0.17	0.09

[a]These results are for the years 1995–1996.

model performs better than both models individually for most years run, including the full 12 years run at once (Table 2). Figure 3 shows the results of this combination model, compared to the low- to high-energy and *Li* [2004] models, for the years 1995–1996.

5. Discussion and Conclusions

[20] The results of this paper demonstrate the effectiveness of a new forecast model that uses a time delay between similar features in low- and high- energy electron fluxes to forecast the logarithm of daily averaged relativistic electron flux at GEO. However, it is not entirely clear what physical process this model represents, and determining the process responsible for the time delay between low- and high-energy electron fluxes is difficult because current theory of both radial diffusion and wave-particle interactions can be used to explain it. The most straightforward explanation for the observed delay is that low-energy electrons are being accelerated locally. However, lower-energy electrons diffuse radially inward at rates higher than those of higher-energy electrons [*Schulz and Lanzerotti*, 1974; *Li et al.*, 2005], and this too can explain the delay observed in the data. The time for inward radial diffusion of MeV electrons to GEO is on the order of days [*Li et al.*, 2001, 2005], and it also takes on the order of 1–2 d for whistler mode chorus to accelerate a seed population of electrons to MeV levels [*Summers and Ma*, 2000; *Horne et al.*, 2005; *Shprits et al.*, 2006; *Bortnik and Thorne*, 2007].

[21] *Horne and Thorne* [1998], *Summers et al.* [1998], and *Meredith et al.* [2002] all agree that the seed population needed for generating MeV electrons due to wave-particle interactions has energy on the order of a few hundred keV, and *Horne et al.* [2005] and *Bortnik and Thorne* [2007] also agree upon a wave-particle interaction cutoff limit at ~300 keV, above which particles are primarily accelerated by the mechanism and below which they are mostly lost by it. These energies correspond to the energies discussed in this paper, but the locations are different. Whistler mode chorus accelerates electrons primarily around L = 4.5 [*Horne et al.*, 2005], but this paper looks at electrons at GEO, where the average L value is ~6. Therefore, if this delay time between low- and high-energy electrons is indeed related to local acceleration by whistler mode chorus, then some outward radial diffusion must be taking place as well in order to explain the similar correlation at GEO.

[22] Despite the ambiguity in determining the physical processes involved, this paper shows that a strong correlation exists between electrons at various energies in the tens of keV to MeV spectrum. This correlation is enhanced when a delay time between low- and high-energy electron fluctuations is incorporated, and, by incorporating this delay time, a new model that forecasts MeV electron flux at GEO has been developed. One of the strengths of this low- to high-energy model is that it relies only on satellites at GEO for input data. By comparison, the *Li* [2004] radial diffusion model needs electron flux data from GEO as well as solar wind measurements from spacecraft at the Sun-Earth L1 point. This L1, single-point reliance increases the risk to the reliability since, if the spacecraft at L1 fails or is shut down, the *Li* [2004] model is rendered inoperable. Thus, having a model that relies only on electron data taken at GEO lowers the risk to potential users because of the multiple spacecraft at GEO that are capable of measuring electron flux.

[23] Conclusions from this study are that a strong, time-dependent correlation exists between daily averaged electron fluxes at different energy levels in the tens of keV to MeV energy spectrum, and this correlation can be used as the basis for a model that accurately forecasts the logarithm of daily averaged MeV electron flux at GEO using only the previous 2 d of electron flux data as input. Such a model has been developed, is working, and can be used for a real-time forecast. Such a forecast can be an important tool for radiation environment risk mitigation for the many spacecraft at GEO. Future work will involve increasing the model's time resolution at GEO [*Burin des Roziers and Li*, 2006], expanding the forecast to other L shells and latitudes, and investigating further the physical processes this model best represents.

[24] **Acknowledgments.** We are indebted to Mike Temerin for his insightful comments and suggestions. We also thank Edward Burin des Roziers and Weichao Tu for helpful discussions and the LANL energetic particles team for their online data access. This work was supported by NSF grants (ATM-0519207, ATM-0549093, and Center for Integrated Space Weather Modeling ATM-0120950). This work was also supported by grants from National Natural Science Foundation of China 40621003 and 40728005.

References

Abel, B., and R. M. Thorne (1998), Electron scattering loss in Earth's inner magnetosphere: 1. Dominant physical processes, *J. Geophys. Res.*, *103*(A2), 2385–2396, doi:10.1029/97JA02919.

Baker, D. (2001), Satellite anomalies due to space storms, in *Space Storms and Space Weather Hazards*, edited by I. A. Daglis, chap. 10, pp. 251–284, Springer, New York.

Baker, D. N., J. H. Allen, S. G. Kanekal, and G. D. Reeves (1998), Disturbed space environment may have been related to pager satellite failure, *Eos Trans. AGU*, *79*(40), 477, doi:10.1029/98EO00359.

Barker, A., X. Li, and R. S. Selesnick (2005), Modeling the radiation belt electrons with radial diffusion driven by the solar wind, *Space Weather*, *3*, S10003, doi:10.1029/2004SW000118.

Bortnik, J., and R. M. Thorne (2007), The dual role of ELF/VLF chorus waves in the acceleration and precipitation of radiation belt electrons, *J. Atmos. Sol. Terr. Phys.*, *69*, 378–386, doi:10.1016/j.jastp.2006.05.030.

Brautigam, D. H., and J. M. Albert (2000), Radial diffusion analysis of outer radiation belt electrons during the October 9, 1990, magnetic storm, *J. Geophys. Res.*, *105*(A1), 291–309, doi:10.1029/1999JA900344.

Burin des Roziers, E., and X. Li (2006), Specification of >2 MeV geosynchronous electrons based on solar wind measurements, *Space Weather*, *4*, S06007, doi:10.1029/2005SW000177.

Chen, Y., G. D. Reeves, and R. H. W. Friedel (2007), The energization of relativistic electrons in the outer Van Allen radiation belt, *Nat. Phys.*, *3*, 614–617, doi:10.1038/nphys655.

Fälthammar, C.-G. (1965), Effects of time-dependent electric fields on geomagnetically trapped radiation, *J. Geophys. Res.*, *70*(11), 2503–2516, doi:10.1029/JZ070i011p02503.

Friedel, R. H. W., G. D. Reeves, and T. Obara (2002), Relativistic electron dynamics in the inner magnetosphere—A review, *J. Atmos. Sol. Terr. Phys.*, *64*, 265–282, doi:10.1016/S1364-6826(01)00088-8.

Gannon, J. L., X. Li, and M. Temerin (2005), Parametric study of shock-induced transport and energization of relativistic electrons in the magnetosphere, *J. Geophys. Res.*, *110*, A12206, doi:10.1029/2004JA010679.

Green, J. C., and M. G. Kivelson (2004), Relativistic electrons in the outer radiation belt: Differentiating between acceleration mechanisms, *J. Geophys. Res.*, *109*, A03213, doi:10.1029/2003JA010153.

Horne, R. B., and R. M. Thorne (1998), Potential waves for relativistic electron scattering and stochastic acceleration during magnetic storms, *Geophys. Res. Lett.*, *25*, 3011–3014, doi:10.1029/98GL01002.

Horne, R. B., R. M. Thorne, S. A. Glauert, J. M. Albert, N. P. Meredith, and R. R. Anderson (2005), Timescale for radiation belt electron acceleration by whistler mode chorus waves, *J. Geophys. Res.*, *110*, A03225, doi:10.1029/2004JA010811.

Hudson, M. K., S. R. Elkington, J. G. Lyon, and C. C. Goodrich (2000), Increase in relativistic electron flux in the inner magnetosphere: ULF wave mode structure, *Adv. Space Res.*, *25*, 2327–2337, doi:10.1016/S0273-1177(99)00518-9.

Li, X. (2004), Variations of 0.7–6.0 MeV electrons at geosynchronous orbit as a function of solar wind, *Space Weather*, *2*, S03006, doi:10.1029/2003SW000017.

Li, X., and M. A. Temerin (2001), The electron radiation belt, *Space Sci. Rev.*, *95*(1–2), 569–580, doi:10.1023/A:1005221108016.

Li, X., I. Roth, M. Temerin, J. R. Wygant, M. K. Hudson, and J. B. Blake (1993), Simulation of the prompt energization and transport of radiation belt particles during the March 24, 1991 SSC, *Geophys. Res. Lett.*, *20*, 2423–2426, doi:10.1029/93GL02701.

Li, X., M. Temerin, D. N. Baker, G. D. Reeves, and D. Larson (2001), Quantitative prediction of radiation belt electrons at geostationary orbit based on solar wind measurements, *Geophys. Res. Lett.*, *28*, 1887–1890, doi:10.1029/2000GL012681.

Li, X., D. N. Baker, S. Elkington, M. Temerin, G. D. Reeves, R. D. Belian, J. B. Blake, H. J. Singer, W. Peria, and G. Parks (2003), Energetic particle injections in the inner magnetosphere as a response to an interplanetary shock, *J. Atmos. Sol. Terr. Phys.*, *65*, 233–244, doi:10.1016/S1364-6826(02)00286-9.

Li, X., D. N. Baker, M. Temerin, G. Reeves, R. Friedel, and C. Shen (2005), Energetic electrons, 50 keV to 6 MeV, at geosynchronous orbit: Their responses to solar wind variations, *Space Weather*, *3*, S04001, doi:10.1029/2004SW000105.

Loto'aniu, T. M., I. R. Mann, L. G. Ozeke, A. A. Chan, Z. C. Dent, and D. K. Milling (2006), Radial diffusion of relativistic electrons into the radiation belt slot region during the 2003 Halloween geomagnetic storms, *J. Geophys. Res.*, *111*, A04218, doi:10.1029/2005JA011355.

Lyons, L. R., R. M. Thorne, and C. F. Kennel (1972), Pitch angle diffusion of radiation belt electrons within the plasmasphere, *J. Geophys. Res.*, *77*(19), 3455–3474, doi:10.1029/JA077i019p03455.

Mann, I. R., T. P. O'Brien, and D. K. Milling (2004), Correlations between ULF wave power, solar wind speed, and relativistic electron flux in the inner magnetosphere: Solar cycle dependence, *J. Atmos. Sol. Terr. Phys.*, *66*, 187–198, doi:10.1016/j.jastp.2003.10.002.

Meredith, N. P., R. B. Horne, R. H. A. Iles, R. M. Thorne, D. Heynderickx, and R. R. Anderson (2002), Outer zone relativistic electron acceleration associated with substorm-enhanced whistler mode chorus, *J. Geophys. Res.*, *107*(A7), 1144, doi:10.1029/2001JA900146.

Millan, R. M., and R. M. Thorne (2007), Review of radiation belt relativistic electron losses, *J. Atmos. Sol. Terr. Phys.*, *69*, 362–377, doi:10.1016/j.jastp.2006.06.019.

O'Brien, T. P., R. L. McPherron, D. Sornette, G. D. Reeves, R. Friedel, and H. J. Singer (2001), Which magnetic storms produce relativistic electrons at geosynchronous orbit?, *J. Geophys. Res.*, *106*(A8), 15,533–15,544, doi:10.1029/2001JA000052.

O'Brien, T. P., K. R. Lorentzen, I. R. Mann, N. P. Meredith, J. B. Blake, J. F. Fennell, M. D. Looper, D. K. Milling, and R. R. Anderson (2003), Energization of relativistic electrons in the presence of ULF power and MeV microbursts: Evidence for dual ULF and VLF acceleration, *J. Geophys. Res.*, *108*(A8), 1329, doi:10.1029/2002JA009784.

Onsager, T. G., J. C. Green, G. D. Reeves, and H. J. Singer (2007), Solar wind and magnetospheric conditions leading to the abrupt loss of outer radiation belt electrons, *J. Geophys. Res.*, *112*, A01202, doi:10.1029/2006JA011708.

Paulikas, G. A., and J. B. Blake (1979), Effects of the solar wind on magnetospheric dynamics: Energetic electrons at the synchronous orbit, in *Quantitative Modeling and Magnetospheric Processes*, *Geophys. Monogr. Ser.*, vol. 21, edited by W. P. Olsen, pp. 180–202, AGU, Washington, D. C.

Reeves, G. D., K. L. McAdams, R. H. W. Friedel, and T. P. O'Brien (2003), Acceleration and loss of relativistic electrons during geomagnetic storms, *Geophys. Res. Lett.*, *30*(10), 1529, doi:10.1029/2002GL016513.

Rostoker, G., S. Skone, and D. N. Baker (1998), On the origin of relativistic electrons in the magnetosphere associated with some geomagnetic storms, *Geophys. Res. Lett.*, *25*, 3701–3704, doi:10.1029/98GL02801.

Roth, I., M. Temerin, and M. K. Hudson (1999), Resonant enhancement of relativistic electron fluxes during geomagnetically active periods, *Ann. Geophys.*, *17*, 631–638, doi:10.1007/s00585-999-0631-2.

Sarris, T. E., X. Li, and M. Temerin (2006), Simulating radial diffusion of energetic (MeV) electrons through a model of fluctuating electric and magnetic fields, *Ann. Geophys.*, *24*, 2583–2598.

Schulz, M., and L. Lanzerotti (1974), *Particle Diffusion in the Radiation Belts*, Springer, New York.

Selesnick, R. S., and J. B. Blake (2000), On the source location of radiation belt relativistic electrons, *J. Geophys. Res.*, *105*(A2), 2607–2624, doi:10.1029/1999JA900445.

Shprits, Y. Y., R. M. Thorne, R. B. Horne, and D. Summers (2006), Bounce-averaged diffusion coefficients for field-aligned chorus waves, *J. Geophys. Res.*, *111*, A10225, doi:10.1029/2006JA011725.

Summers, D., and C. Ma (2000), A model for generating relativistic electrons in the Earth's inner magnetosphere based on gyroresonant wave-particle interactions, *J. Geophys. Res.*, *105*(A2), 2625–2639, doi:10.1029/1999JA900444.

Summers, D., R. M. Thorne, and F. Xiao (1998), Relativistic theory of wave-particle resonant diffusion with application to electron acceleration in the magnetosphere, *J. Geophys. Res.*, *103*(A9), 20,487–20,500, doi:10.1029/98JA01740.

Temerin, M., I. Roth, M. K. Hudson, and J. R. Wygant (1994), New paradigm for the transport and energization of radiation belt particles, *Eos Trans. AGU*, *75*(44), Fall Meet. Suppl., 538.

Williams, D. J. (1966), A 27-day periodicity in outer zone trapped electron intensities, *J. Geophys. Res.*, *71*(7), 1815–1826.

X. Li and D. L. Turner, Laboratory for Atmospheric and Space Physics, University of Colorado, 1234 Innovation Drive, Boulder, CO 80303, USA. (drew.lawson.turner@gmail.com)